Tuning the lasing frequency and reducing the laser Linewidth of GaAs Semiconductor Laser Using External Oscillating Driving Field

Dr. Hassan S. Ashour *

الملخص

في هذه الدراسة، نحن نقترح طريقة جديدة لتغيير الطول الموجي لشعاع الليزر وتقليل الاتساع الطيفي المنبعث من ليزر أشباه الموصلات باستخدام مجال خارجي. استخدمنا طريقة فوكالات التي تعين احتمالية المرور للالكترونات الساقطة على جهد متردد والتي تعين شكل ومكان أشباه الحالات المرتبطة. قمنا بحل مصفوفة المرور لفوكالات عدديا. ولقد وجدنا أن سعة المجال V_1 تلعب دور أساسي في تحديد شكل تجمع الالكترونات في أشباه الحالات المرتبطة وأيضا شدة المجال تلعب دور مهم في مكان حدوث أشباه الحالات المرتبطة على محور الطاقة. هذه الإزاحة في موضع أشباه الحالات المرتبطة جعلت من الممكن تغيير تردد شعاع الليزر وتقليل اتساع طيف الليزر يتم بتغيير سعة المجال الساقط على ليزر أشباه الموصلات.

ABSTRACT

In this paper, we propose a new method to tune intrinsic GaAs semiconductor laser lasing frequency and reducing the laser linewidth using an external deriving field. We used the developed Floquet S-matrix which determines the transmission probabilities and the shape and position of the induced quasibound state, which accumulated incident electrons. We solve the S-matrix numerically to the system parameters. We found that the oscillating field amplitude V_1 plays a curial rule in defining the profile of electrons accumulations in the quasibound state, and the field's strength made shift the position of the quasibound state. This shift in the bound state energy due field's strength is used to tune the lasing frequency and the output of the semiconductor laser linewidth is improved by changing the field's amplitude the deriving field.

Keywords: Semiconductor laser, tunable laser, laser linewidth

* Department of Physics, Faculty of Applied Sciences, Al-Azhar University-Gaza, Palestine, Email: hashour@alazhar-gaza.edu.

INTRODUCTION:

Tunable lasers are different from the traditional lasers because their output frequency, color, in a given spectral range can be changed. These quantum devices found numerous applications in many diverse fields. Among the fields that employ tunable lasers are: laser cooling, atomic physics, communication, imaging, medicine, remote sensing, etc. Tunable laser, were discovered by Sorokin et al [1] and Schafer et al [2] in 1966, is a dye laser. A significant advance toward emission control was provided by Peterson et al [3] in 1970. However, these lasers were not compact and required a large two-dimensional diffraction grating. Resonator laser designed to yield tunable narrow linewidth emission in compact and improved configurations are the grazing-incident cavities [4-6] and the multiple-prism grating oscillators [7-9]. These cavity designs have been successful in tuning and frequency narrowing in gas lasers, solid-state lasers, and semiconductor lasers.

Semiconductor lasers are vastly used in dense wavelength division multiplexing (DWDM) networks, including wavelength conversion, optical routing and multi-wavelength sparing. Many techniques currently being investigated to produce such lasers [10-15]: external cavity diode lasers (ECL) offer significant advantages, including wide tuning ranges, high output power, narrow linewidths with good side mode suppression and accurate wavelength control. These devices are widely used in test equipment, but the size and complexity of the optomechanical assemblies have limited their use in optical Networks [4]. The use of silicon Micro-Electro-Mechanical Systems (MEMS) to perform the mechanical tuning functions makes it possible to greatly reduce the size and complexity of the devices, and combining the ECL and an etalon wavelength locker (WLL) in the same package results in a compact, robust device suitable for use in optical networks. [16]

Wenjun and Reichl and others [17-21] studied the electron scattering through time periodic potential well using Floquet S-matrix. In their study they found that the oscillator-induced quasibound states can accumulate electrons and give rise to electrons interchannel transitions at resonance. The transmission resonances result from the interaction of electrons with the oscillating field. Also, the applied field causes the bound state of the quantum well to be shifted by a certain amount because of this interaction. In this paper, we utilized and improved their result to tune the semiconductor laser diode.

This paper is organized as follow: in section 2, we briefly introduced the bound state in quantum well; and then we introduce Floquet scattering matrix for quantum well, then the S-matrix structured and used numerically to calculate the transmissions probabilities with various system parameters. In section 3, we propose a method to tune the semiconductor laser lasing frequency and improving the output frequency using an external deriving field. Section 4 is devoted to the conclusion.

2. Theory:

2.a Bound state

For GaAs finite square well potential, quantum well, the potential is given by [22]

$$V(x)=\begin{cases} -V_0 & |x| \geq a \\ 0 & |x| < a \end{cases}, \qquad (2.1.1)$$

The Schrödinger wave equation is

$$\left[-\frac{d}{dx}\frac{1}{m}\frac{d}{x}+V(x)\right]\psi(x)=E\psi(x), \qquad (2.1.2)$$

Where $m=m_1^*$ in the well region and in the barrier region. Here, we are going to consider the bound state solution which have energies in the range between 0 and V_0.

Solving equation (2.1.2) in the well and barrier regions and applying the boundary conditions, we can find the eigenenergies E. In general, the solutions leads to a quantized eigenenergies [22]

$$\left(\tan ka - \frac{b}{k}\right)\left(\tan ka + \frac{k}{b}\right) = 0 \qquad (2.1.3)$$

Thus $k=\sqrt{\frac{2m(E+V_0)}{\hbar^2}}$, and $b=\sqrt{\frac{2m|E|}{\hbar^2}}$. Equation (2.1.3) can be solved numerically by any CAD tools, like Maple or Matlab, to obtain the energy eigenvalues and correspondingly the allowed bound states in the quantum well.

2.b Floquet Scattering:

When an external oscillating field with frequency ω and amplitude V_1 is applied on the GaAs quantum well, as in figure 1, the Schrödinger wave equation can be written as

$$i\hbar\frac{\partial}{\partial t}\psi(x,t)=-\frac{\hbar^2}{2m_1^*}\frac{\partial^2}{\partial^2 x^2}\psi(x,t)+V(x,t)\psi(x,t), \qquad (2.2.1)$$

Thus m_1^* is the electron's effective mass in the well region, and $V(x,t)$ is the total field given by

$$V(x,t)=\begin{cases}0 & x>L/2\\ V_0+V_1\cos(\omega t) & -L/2<x<L/2,\\ 0 & -L/2>x\end{cases} \qquad (2.2.2)$$

Thus L is the quantum well width, and V_1 is the field strength.

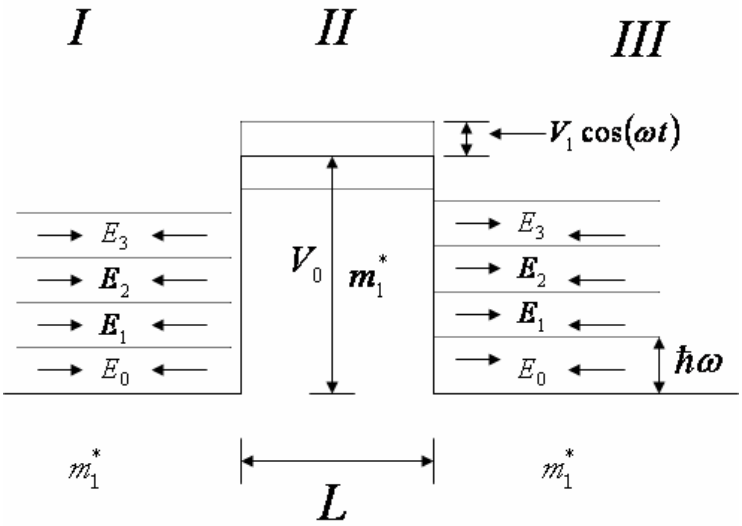

Figure 1: Floquet scattering model. The incoming electrons and backscattered electrons in channels are spaced by field strength $\hbar\omega$. Floquet channels are spaced according to $E_n = E_0 + n\hbar\omega \;\; [n \in [0,\infty)]$.

The evanescent mode exists but not included in the figure.

In this treatment, we neglected electron-electron interaction, and we assume the temperature is low enough so that electron-phonon interaction can be neglected as well. We assumed the scattering of electrons mainly from the geometrical structure of the potential.

According to Floquet theorem equation (2.1) has a solution of the form [20]

$$\psi_F(x,t)=e^{-iE_Ft/\hbar}\phi(x,t), \qquad (2.2.3)$$

Thus E_F is the Floquet energy that can be determined from the boundary conditions. We need to solve Schrödinger wave equation (2.1) for each layer then apply the boundary conditions between the adjacent layers. The Floquet state, $\psi_{II}(x,t)$, inside the oscillating quantum well is given by

$$\psi_{II}(x,t)=e^{-iE_Ft/\hbar}\sum_{n=-\infty}^{\infty}\sum_{m=-\infty}^{\infty}\left(a_m e^{iq_m x}+b_m e^{-iq_m x}\right)J_{n-m}\left(\frac{V_1}{\hbar\omega}\right)e^{-in\omega t}, \qquad (2.2.4)$$

Thus a_m and b_m are constant coefficients to be determined from the boundary conditions and q_m can be found from the following relation

$$\frac{\hbar^2 q_m^2}{2m_1^*} = E_F + m\hbar\omega - V_0, \tag{2.2.5}$$

When a beam of electrons is incident on the oscillating quantum well the electrons will be scattered inelastically into Floquet side bands. In order to be able to apply the boundary conditions between the oscillating quantum well and the adjacent regions the wave function outside the quantum well must consist of many Floquet side bands. The solution of Schrödinger wave equation outside the oscillating quantum well, in regions I and III, is given by

$$\psi^{I}(x,t) = \sum_{n=-\infty}^{\infty}\left(A_n^i\, e^{(ik_n x - iE_n t/\hbar)} + A_n^o\, e^{(-ik_n - iE_n t/\hbar)}\right), \tag{2.2.6}$$

$$\psi^{II}(x,t) = \sum_{n=-\infty}^{\infty}\left(B_n^i\, e^{(-ik_n x - iE_n t/\hbar)} + B_n^o\, e^{(ik_n - iE_n t/\hbar)}\right), \tag{2.2.7}$$

Thus A_n^i and B_n^i are the probability amplitudes of the incoming waves from the left and right, respectively, while A_n^o and B_n^o are the probability amplitudes of the outgoing waves. The incoming and outgoing waves are divided into different zones according to channel index n: $E_n = E_0 + n\hbar\omega$, where E_0 is the Floquet energy of the propagating mode with the lowest energy [17-19]. Also, it is important to mention that $k_n = \sqrt{2m_1^* E_n/\hbar^2}$. However, when $E_n < 0, k_n = \sqrt{2m_1^* E_n/\hbar^2}$ is imaginary, such a mode represents a non-propagate and is called evanescent mode.

The Floquet Scattering matrix could be obtained; the derivation is given in [20], using equations (2.4), (2.6), and (2.7). That is

$$\begin{pmatrix} A^o \\ B^o \end{pmatrix} = S \begin{pmatrix} A^i \\ B^i \end{pmatrix}, \tag{2.2.8}$$

The S matrix consists of all the probability amplitudes which connect the coefficients A_n^i, B_n^i to the coefficients A_n^o, B_n^o. The structure of the S-matrix is

$$S = \begin{pmatrix} M_{AA} & M_{AB} \\ M_{BA} & M_{BB} \end{pmatrix}, \tag{2.2.9}$$

Where the elements $M_{AA}, M_{AB,}\, M_{BA,}$ and M_{BB} are given by

$$M_{AA}=\frac{1}{2}\left\{M_c^{+}\cdot\left[\left(M_s^{+}\right)^{-1}+\left(M_s^{-}\right)^{-1}\right]+M_c^{-}\left[\left(M_s^{+}\right)^{-1}-\left(M_s^{-}\right)^{-1}\right]\right\}\cdot M_r-M_i, \quad (2.2.10.a)$$

$$M_{AB}=\frac{1}{2}\left\{M_c^{+}\cdot\left[\left(M_s^{+}\right)^{-1}-\left(M_s^{-}\right)^{-1}\right]+M_c^{-}\left[\left(M_s^{+}\right)^{-1}+\left(M_s^{-}\right)^{-1}\right]\right\}\cdot M_r, \quad (2.2.10.b)$$

$$M_{BA}=\frac{1}{2}\left\{M_c^{-}\cdot\left[\left(M_s^{+}\right)^{-1}+\left(M_s^{-}\right)^{-1}\right]+M_c^{+}\left[\left(M_s^{+}\right)^{-1}-\left(M_s^{-}\right)^{-1}\right]\right\}\cdot M_r \quad (2.2.10.c)$$

$$M_{BB}=\frac{1}{2}\left\{M_c^{-}\cdot\left[\left(M_s^{+}\right)^{-1}-\left(M_s^{-}\right)^{-1}\right]+M_c^{+}\left[\left(M_s^{+}\right)^{-1}+\left(M_s^{-}\right)^{-1}\right]\right\}\cdot M_r-M_i, \quad (2.2.10.d)$$

Where

$$M_s^{\pm}=\left[\left(k_n+q_m\right)e^{-iq_mL/2}\pm\left(k_n-q_m\right)e^{iq_mL/2}\right]J_{n-m}\left(\frac{V_1}{\hbar\omega}\right), \quad (2.2.11.a)$$

$$M_r=2k_ne^{-ik_nL/2}\delta_{n,m}, \quad (2.2.11.b)$$

$$M_c^{\pm}=e^{-i\left(k_n\pm q_m\right)L/2}J_{n-m}\left(\frac{V_1}{\hbar\omega}\right), \quad (2.2.11.c)$$

$$M_i=e^{-ik_nL}\delta_{n,m.} \quad (2.2.11.d)$$

In the S-matrix each element gives the probability amplitude of electron scattered from Floquet sideband m to sideband n $\left[n,m\in\left(-\infty,\infty\right)\right]$.

The S-matrix of the incoming and outgoing Floquet sidebands is in the following form

$$S=\begin{pmatrix} r_{00} & r_{01} & . & . & t_{00}^{'} & t_{01}^{'} & . & . \\ r_{10} & r_{11} & . & . & t_{10}^{'} & t_{11}^{'} & . & . \\ . & . & . & . & . & . & . & . \\ . & . & . & . & . & . & . & . \\ t_{00} & t_{01} & . & . & r_{00}^{'} & r_{01}^{'} & . & . \\ t_{01} & t_{11} & . & . & r_{10}^{'} & r_{11}^{'} & . & . \\ . & . & . & . & . & . & . & . \\ . & . & . & . & . & . & . & . \end{pmatrix}. \quad (2.2.12)$$

Where r_{nm} and t_{nm} are the reflection and transmission coefficients, respectively, for modes incident from left; $r_{nm}^{'}$ and $t_{nm}^{'}$, and for modes incident from right; r_{nm} and t_{nm}. The other modes like $t_{-1,0}, r_{-1,0}$ in the S-matrix, does not appearing in equation 2.12, correspond to probability amplitude describing an electron with incident energy E_0 being scattered into the evanescent mode $E_{-1}=E_0-\hbar\omega$. In other word, the electron lost a quanta of $\hbar\omega$ upon its interaction with the oscillating quantum well.

From the scattering S-matrix the total transmission coefficient can be obtained

$$T = \sum_{n=0}^{\infty}\sum_{m=0}^{\infty}\frac{k_n}{k_m}\left|t_{nm}\right|^2 \qquad (2.2.13)$$

According to Landuar-Büttiker formula [22-24] the total conductance, which can be measured experimentally, is given by

$$G = \frac{2e^2}{h}T \qquad (2.2.14)$$

In the numerical simulation, the minimum number of sidebands, channels, is determined by the strength of the oscillation according to [17, 21]

$$N \cong V_1/\hbar\omega \qquad (2.2.15)$$

The numerical routine showed some deviation from equation (2.2.15).We took this deviation into consideration by monitoring the probability of each channel. Then, we can decide if the number of channels included is enough or not.In figure2 we numerically find the transmission trough oscillating quantum well using the following parameters which were used in reference [20]:

$V_0 = -20\,meV$, $V_1 = 5\,meV$, $L = 10A^{\circ}$, $m_1^* = 0.067\,m_e$, and $\hbar\omega = 1\ meV$.

According to equation 2.15, we need 5 sidebands to take into account. So, the all over sidebands in the scattering pattern is 11; 5 above the incident energy and 5 below the incident energy. The energy of each sideband is given by $E_n = E_0 + n\hbar\omega$ with $n = 0,\pm1,.....,\pm N$, and $N = 5$.

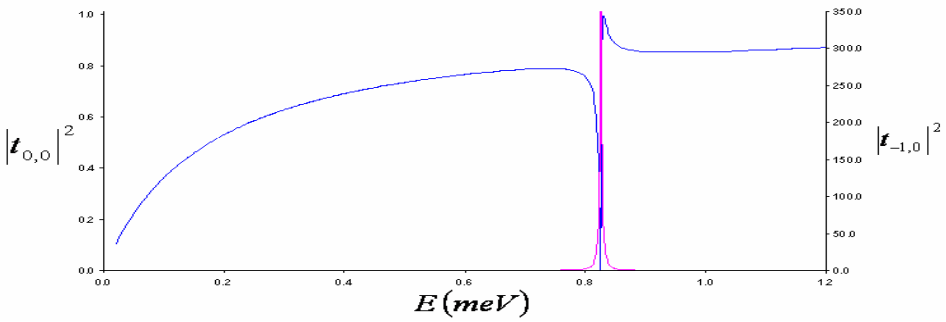

Figure2: The Transmission coefficient T as a function of the incident energy for the listed above system parameters, the solid line. The secondary axis shows the accumulation of electrons in quasi bound state.

As it can be seen in figure 2, the transmission has a dip followed by a sharp increase in the transmission at specific energy value. This is called asymmetric Fano resonance [17] at $E = 0.826\ meV$, $(E = \hbar w - |E_B| \approx 0.826 meV)$, where E_B is the bound state energy when

$V_1 = 0$ which equals - $0.174 meV$. This dip is occurred when the difference between the incident electron energy and the bound state is equal to $\hbar\omega, 2\hbar\omega, ...$

In figure 3, we explore the effect of the oscillating frequency, $\hbar\omega$, on the transmission pattern. The number of channels included in this figure is according to equation 2.2.15. In figure 3-a, we plot the transmission coefficient versus electron's incident energy with different values of $\hbar\omega$ .The first curve resonance occurs at $0.32 meV$ with field incident energy is $0.5\hbar\omega$, the second curve resonance occurs at $0.826 meV$ when the incident field energy is $\hbar\omega$, and the third curve resonance occurs at $1.36 meV$ for the incident field energy $1.5\hbar\omega$. In figure 3-b, we show the electrons accumulation in the quasibound state which occurs where the resonance occurred. Notice, the higher the energy of the oscillating filed energy is the higher the quasibound states that can be accumulate electrons.

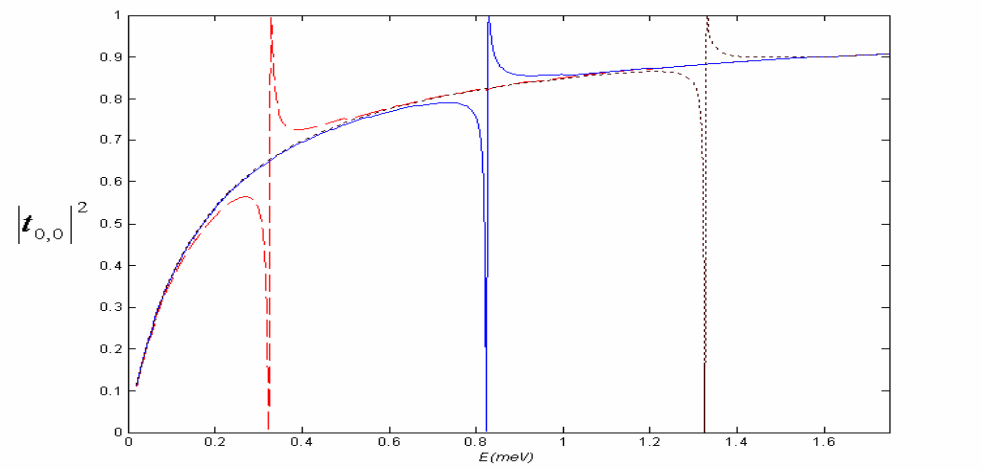

Figure 3-a: The transmission coefficient T as function of incident energy for different oscillating field energies. Curve 1(dashed) with $0.5\hbar\omega$, curve 2 (solid) with $\hbar\omega$, and curve 3 (dotted) with $1.5\hbar\omega$.

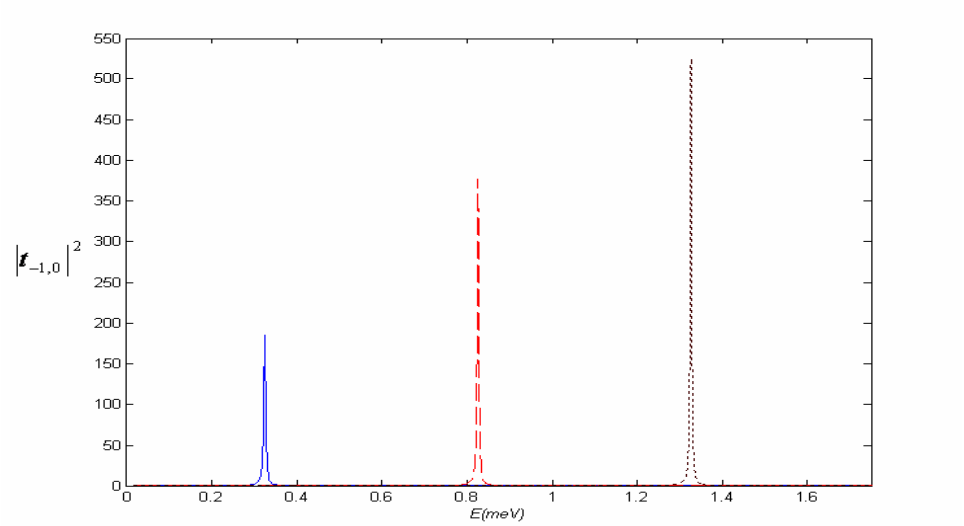

Figure 3-b: The accumulation of electrons in the quasi bound state induced by the oscillating driving field with energies listed in figure 3-a.

In figure 4, we studied the effect of the strength of the oscillating field, V_1, on the electronic transmission through the oscillating quantum well . The number of channels included to reach this figure is given by equation 2.2.15, which ranges between seven to fifteen channels. The system of parameters are $V_0 = -20\,meV$, $L = 10A^{\circ}$, $m_1^* = 0.067\,m_e$, and $\hbar\omega = 1\ meV$. In figure 4-a, we plot the transmission T versus the incident electron energy but with different amplitudes of the incident deriving field. We notice an increase in the asymmetric Fano resonance widen with increasing V_1. In figure 4-b, we plot the accumulation of electrons in the quasibound state. The quasibound state is sharper when V_1 is small but it is broader when V_1 takes high values. This broad quasibound state gives high uncertainty in electron's energy piled up in the quasibound state. Ironically, the increase in the field's amplitude leads to broad quasibound state, figures 4-b and 4-c, and less electron accumulation in the quasi bound state. Also, we noticed that the position of the quasibound state displaced to lower energy values when the amplitude V_1 is displaced to higher values. This shift in the position of the quasibound state is not predicted by [20], and for the moment we cannot give a reasonable explanation for this behavior.

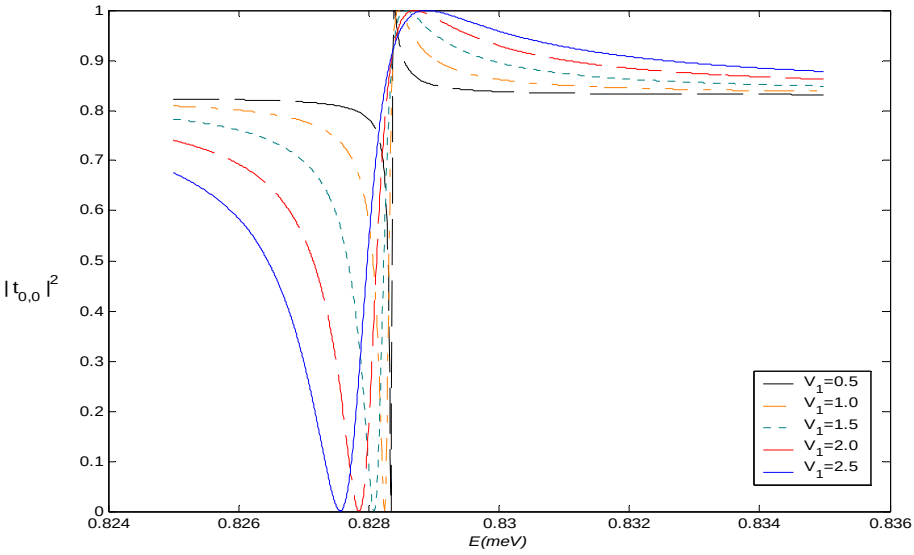

Figure 4-a: The transmission coefficient T as a function of the incident energy for different oscillating field amplitudes listed in the figure legends in units meV.

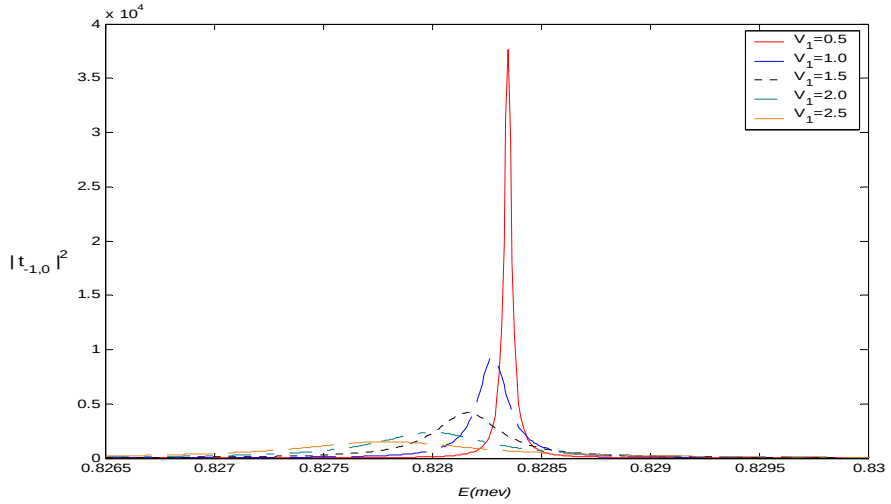

Figure 4-b: The accumulation of electrons in the quasi bound state induced by the oscillating driving field amplitudes that are listed in the figure legend in meV.

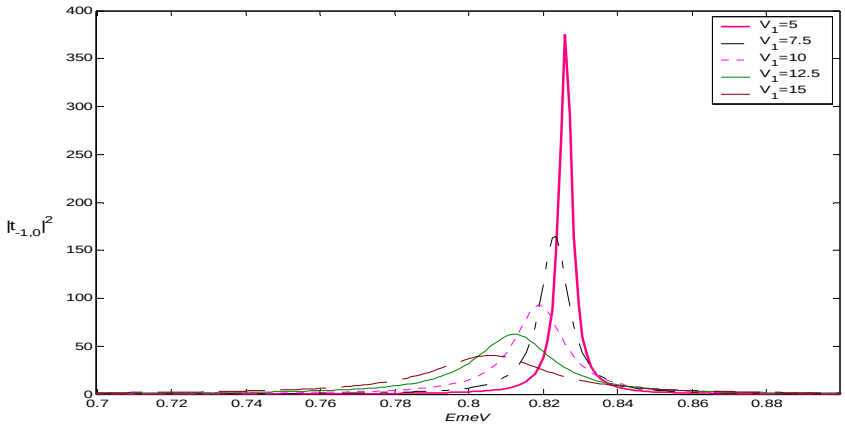

Figure 4-c: The accumulation of electrons in the quasi bound state induced by the oscillating driving field amplitudes that are listed in the figure legend in meV.

Here, we will utilize all the information gained from the above figures. If we want a sharp and high accumulation for electrons, we need to use high values for the oscillating field energy, $\hbar\omega$, and law field amplitude values. The position of the quasibound state can be shifted by changing the field energy, but once the device is fabricated the only parameters that can be used to control over are the field energy and the amplitude. In figure 5(a and b), we plot the transmission and the electron accumulations for the following system of parameters: $V_0 = -20$, $m_1^* = 0.067m_e$, $\hbar\omega = 1.5meV$, and $V_1 = 0.5meV$

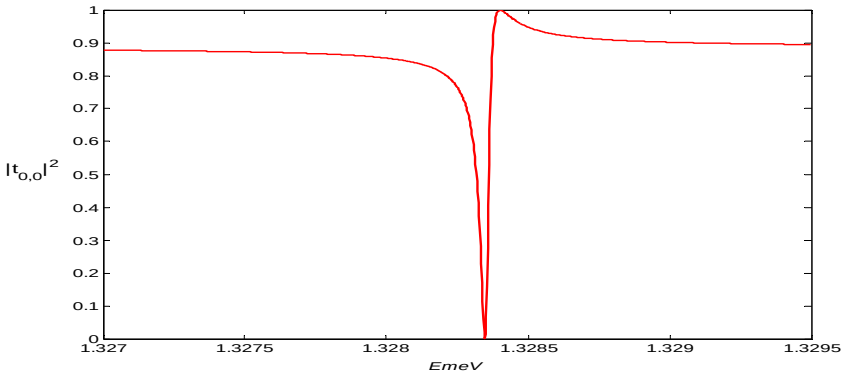

Figure 5-a: The transmission coefficient T as function of incident energy for the following system parameters: $V_0 = -20$, $m_1^* = 0.067m_e$, $\hbar\omega = 1.5meV$ **, and** $V_1 = 0.5meV$

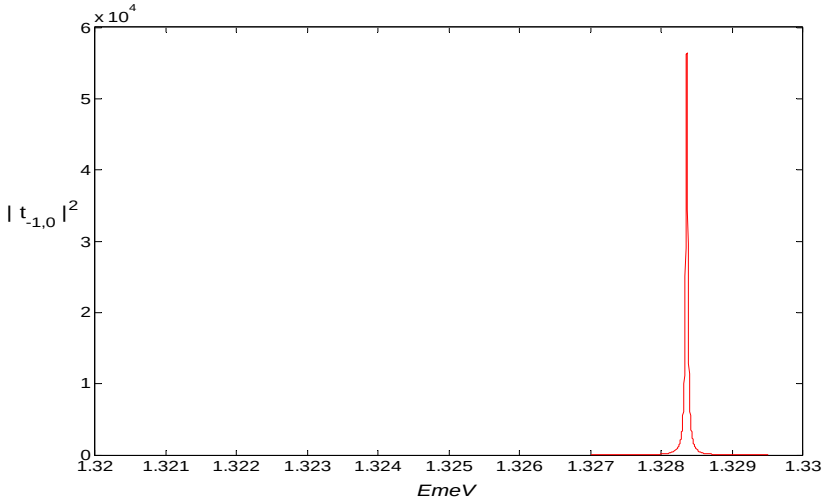

Figure 5-b: The accumulation of electrons in the quasi bound state induced by the oscillating driving field amplitude with the system of parameters that are listed in figure 5-a.

3. Tuning the SCL :

We describe a simple form of semiconductor laser diode [23-30] and the references therein. The semiconductor laser structured from a thin layer $(0.1 \sim 0.2\mu m)$ of GaAs which is sandwiched between two layers of $Ga_{1-x}Al_xAs$ of opposite doping forming a double heterojunction. Figure 6 shows the energy band structure of a diode laser. Figure 6, shows the conduction and valance band edges in a heterojunction diode at full forward bias. In this structure a potential well of electrons of height ΔE_c which coincides spatially with a well for holes of height ΔE_v. In other word, we have a direct band gap structure which is recommended for light generation devices. Under forward bias with $eV_a \sim E_g$, where V_a is the applied voltage and E_g is the energy gap, the large densities of injected electrons from the n side and holes from the p side in the well, causes the inversion condition, given by

$$E_{Fc} - E_{Fv} > \hbar\omega \qquad (3.1)$$

Where E_{Fc}, and E_{Fv} are the quasi-Fermi energies for electrons in the conduction band and holes in the valence band, respectively, and $\hbar\omega$, the photon's energy in electron volts, where ω is the lasing frequency.

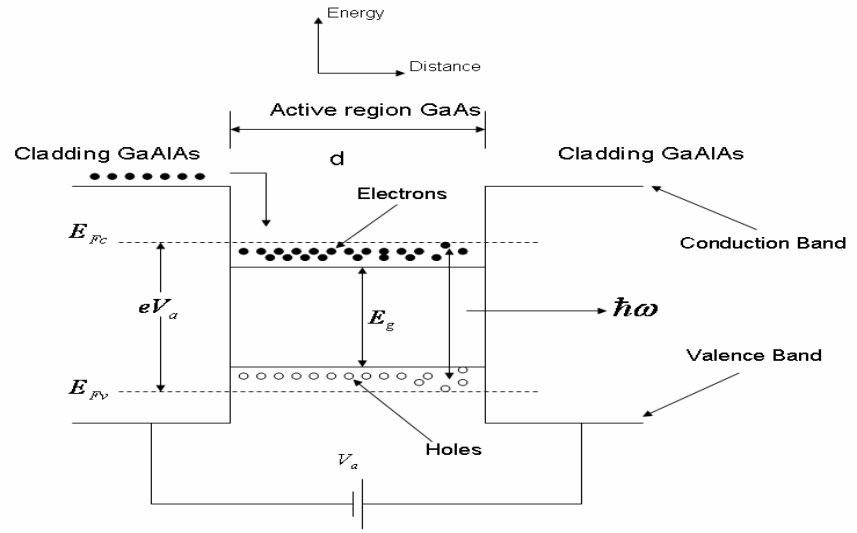

Figure 6: Schematic diagram of a semiconductor laser diode. The conduction and valence band edges under positive bias in a double heterojunction GaAlAs/GaAs/GaAlAs laser diode. The black circles is electrons and the hollow circle is the holes.

The GaAs inner layer, where stimulated emission takes place, is called the active region. To maintain the lasing action of the gain medium, it is necessary to confine the light as tightly as possible to the active region. Since the walk away modes does not contribute to the gain. This confinement can be achieved by dielectric waveguiding effect due the dielectric constant difference between the gain medium and the barrier regions. When the optical mode is confined to the active region the diode laser lases at frequency ω with photon energy,

$$\hbar\omega = E_{Fc} - E_{Fv}. \tag{3.2}$$

From the discussion in section 2, we know that the effect of the oscillating driving field causes the bound state to be shifted by a significant energy value to form a quasibound state. The gain region under the effect of oscillating deriving field would cause the energy difference between the quasi-Fermi energy levels for electrons and holes to widen out. Thus, the laser frequency tuned to higher frequency values which changes the laser diode output frequency,

$$\hbar\omega' = E'_{Fc} - E'_{Ev} \tag{3.3}$$

Where ω' is the new lasing frequency, and E'_{Fc} and E'_{Ev} are the new quasi-Fermi energy levels for electron in the conduction band and for hole in the

valence band, respectively, under the presence of the external oscillating driving field. Another possible refinement of the laser operations is to lower the laser linewidth and increasing its monochromaticity. This happens, when the electrons piled in the quasibound state, but according the system parameters this pile of electrons can be sharp or wide over a significant energy interval, see figures 4-b and 5-b. For a good laser operation it is desirable to confine electrons in a very narrow energy band. This confinement would lead to lower laser linewidth and would increase the monochromaticity of the laser diode output. The laser intensity can be controlled by controlling the number of electrons can be trapped in the quasibound state. Once the laser diode is fabricated cannot control neither the effective masses of the well nor the barrier regions. In figure 5-b, the controlling factor of the height and width of the quasibound state is the oscillating field amplitude V_1, the quasibound state has almost the same position in energy which means the lasing frequency would not change significantly with changing the field amplitude, however the intensity does.

CONCLUSION:

We developed Floquet scattering theory to determine the scattering matrix, S-matrix, for oscillating quantum well driven by external field. By numerically solving the S-matrix, we were able to determine the quasibound state induced because of the oscillating driving field and the profile of the electron accumulation in the quasibound state. Also, with the aid of the numerical code, we were able to study the effect of the system's parameter of the transmission amplitude. We found out that the most important parameters of the system are the field energy and field amplitude, which we can control. The physical parameters of the semiconductor diode we cannot be controlled once the device is fabricated. The shift detected in the bound state energy is used to tune the lasing frequency and the output laser linewidth of the semiconductor laser by changing the deriving field frequency and amplitude.

ACKNOWLEDGEMENT:

The author wishes to thanks Dr. Ahmed El-Tayyan for a helpful discussion and fine comments on the subject of this paper.

REFERENCES:

1. P. P. Sorokin and J. R. Lankard, Stimulated emission obseverd from an organic dye, chloro-aluminum phthalocyanine, IBM J. Res. Develop. 10, 162-163 (1966).

2. F. P. Schafer, W. Schmidt, and J. Volze, Organic dye solution laser, Appl. Phys. Lett. 9, 306-309 (1966).
3. O. G. Peterson, S. A. Tuccio, and B. B. Snavely, CW operation of an organic dye solution laser, Appl. Phys. Lett. 17, 245-247 (1970)
4. I. Shoshan, N. N. Danon, and U. P. Oppenheim, Narrowband operation of a pulsed dye laser without intracavity beam expansion, J. Appl. Phys. 48, 5595-4497 (1997)
5. M. G. Littman and H. J. Metcalf, Spectrally narrow pulsed dye laser without beam expander, App. Opt. 17, 2224-2227 (1978)
6. M. G. Littman, Single-mode pulsed tunable dye laser, App. Opt. 23, 4465-4468 (1984).
7. F. J. Durate and J. A. Piper, A double-prism beam expander for pulsed dye laser, Opt. Commun. 35, 100-104 (1980)
8. F. J. Durate and J. A. Piper, Prism preexpanded grazing-incidence grating cavity for pulsed dye lasers, Appl. Opt. 21, 2113-2116 (1981).
9. F. J. Durate and J. A. Piper, Narrow-linewidth, high prf copper laser-pumped dye-laser oscillators, Appl. Opt. 23, 1391-1394 (1984).
10. Jin Hong, Hyung Kim, and Toshi Makino, Enhanced wavelength tuning range in two-section complex-coupled DFB lasers by alternating gain and loss coupling, IEEE J. Light. Tech. 16, 1323-1328 (1998).
11. B. Mason, G.A. Fish, S.P. DenBaars, and L.A. Coldren, Widely tunable sampled grating DBR laser with integrated electroabsorption modulator, Photon. Tech. Lett. 11, 638-640 (1999).
12. D. Vakhshoori, P. Tayebati, Chih-Cheng Lu, M. Azimi, P. Wang, Jiang-Huai Zhou and E. Canoglu, 2 mW CW single mode operation of a tunable 1550 nm vertical cavity surface emitting laser with 50 nm tuning range, Electron. Lett. 35, 1-2 (1999).
13. T. Day, F. Luecke, and M. Brownell, Continuously tunable diode lasers, Lasers and Optronics , June (1993).
14. P. Zorabedian, Tunable External Cavity Semiconductor Lasers, in Tunable Laser Handbook, (F.J. Duarte Ed.), Academic Press, San Diego, (1995).
15. J.H. Jerman, J.D. Grade, J.D. Berger, and J.H. Heanue, Tunable Laser with Microactuator, Int. Pub. No. WO 01/43241, June, (2001).

16. P. Zorabedian, Tunable External Cavity Semiconductor Lasers, in Tunable Laser Handbook, (F.J. Duarte Ed.), Academic Press, San Diego, (1995).
17. Wenjun Li, and L. E. Reichl, Floquet scattering through a time periodic potential, Phys. Rev. B 60, 15 732 (1999).
18. M. Moskalets and M. Büttiker, Floquet states and persistent currents transitions in a mesoscopic ring, arXiv:cond-mat/0207258 v1 10 July 2002.
19. M. Moskalets and M. Büttiker, Floquet scattering theory of quantum pumps, arXiv:cond-matt/0208356 v1 19 Aug 2002 Kyungsun Na, and L.E. Reichl, Effect of the quasibound states on quantum transport in a ballistic electron waveguide, Phys Rev B 59, 13073 (1998)
20. Wenjun Li, and L. E. Reichl, Transport in strongly driven heterostructures and bound state induced dynamic resonances, Phys. Rev B 62, 8269 (2000).
21. C. S. Tang, Y. H. Tan, and C. S. Chu, Transport spectroscopy in a time-modulated open quantum dot, Phys. Rev B 67, 205324-1 (2003).
22. Amit Goaswami, Quantum Mechanics, WCB, 1997.
23. Shun Lien Chuang, Physics of Optoelectronic Devices, Wiley series in pure and Applies physics, (1995).
24. Liboff, Qunatum Mechanics,2nd edition Addison-Wesley (1993), P. 685-691 .
25. M. Büttiker, Phys. Rev. Lett. 57, 1761 (1986).
26. R. Landauer, J. Phys.: Condend. Matter 1, 8099 (1989).
27. G. P. Berman, E. N. Bulgakov, D. K. Campbell, and A. F. Sadreev, Physica B 225, 1 (1996).
28. Amnon Yariv, Quantum Electronics, 3rd edition, Wiley (1989), p264-276.
29. Chow, Koch, and Sargent III, Semiconductor laser physics, Springer-Verlag (1994).
30. J. T. Verdeyen, Laser Electronics, 3rd edition, Prentice Hall (1995), P.440-500.